Laboratory of Applied Mathematics and Mechanics

Simulation of Turbulent Diffusion Flames

Author: Alex Frolov
E-mail: frolovalex@list.ru
ICQ: 285-819-243

Contents

Introduction

The problem of this report arose in the context of the FireEx fire-fighting project that is in progress in the laboratory of Applied Mathematics and Mechanics of Saint-Petersburg State Polytechnical University.

This project is aimed at simulating turbulent diffusion flames on different combinations of physical models. It was decided to make all the simulations (in the network of this problem) on commercial software with comprehensive facilities, and Fluent was chosen to be this software. The main aim of these simulations is to obtain a wide picture of the applicability of different turbulent, chemistry and radiation models to the problem of turbulent diffusive flames.

To test reliability of these simulations a special well documented and researched flame was chosen with a quite complete experimental data available. The flame is from Sandia National Laboratories Archive (Sandia National Laboratories, California) and is called Sandia Piloted Flame D. It is a methane-air diffusive flame with pilot-stabilizer. Pilot is an additional surrounding annulus flame of the same composition (no violation on global composition) to stabilize the main flame and prevent its breakaway.

The pilot is modelled as the combustion products at specified temperature.

1 Problem Statement

1.1 Physical Statement

The burner of Sandia Piloted Flame D is situated on an axis of a vertical wind tunnel with dimensions 30 cm by 30 cm. The orientation of the burner is parallel to the wind tunnel axis. The burner has the following dimensions. The main jet diameter is *d=7.2* mm, and this is the characteristic length unit for this problem. The pilot annulus inner diameter is *7.7 mm* and outer diameter is *18.2 mm*. Finally, burner outer wall diameter is *18.9 mm*. Visible length if the flame is about *67d*.

1.2 Computational Statement

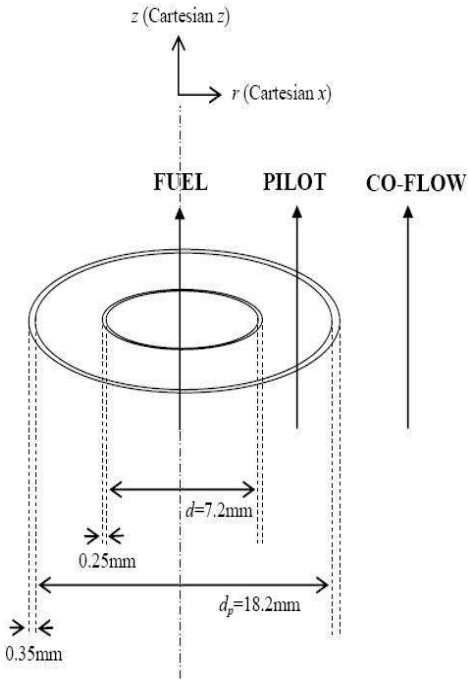

The computational is modelled as an inverted and truncated cone with the following dimensions. The lower cone base diameter is *6d* and the burner is located in the centre of this base. The greater cone base diameter is *38d*, and the truncated cone height is *80d*.

Lets consider boundary conditions of the problem.

Velocity boundary conditions are the following. The main velocity magnitude of the main jet is 49.6 m/s. The main velocity magnitude of the pilot bulk is 11.4 m/s. The main velocity of surrounding co-flow is 0.9 m/s. To be honest it is necessary to say that these are the mean values. Actually the velocity magnitude profile is used.

The temperature boundary conditions are 294, 1880 and 291 K for main jet, pilot bulk and co-flow correspondingly. The composition boundary conditions are the following. Main jet is represented as 25% CH4 and 75% air (partially premixed) by volume (by moles). Co-flow composition is 100% air. And the pilot composition is an experimental data, that is presented in two ways: in terms of mass fractions for each element in composition and in term of mixture fraction.

2 Physical models

2.1 Fluid flow field equations

Navier-Stokes equations for multi-component reacting medium are used for combustion problems. In such type of problems we are interested in for distribution fields for each component of the mixture. So in this system we have additional transport equations for each component. It is a good idea to imagine that a whole medium described by continuity equation is split into a sum of several components with its own transport equation. This way, if we sum all these equation, we'll obtain a continuity equation (these equations are linear-dependent). And of course, the combustion problems are highly temperature-dependent, so energy transport equation is included in this system (for combustion problem this equation is written in enthalpy terms).

The whole equation system has the following representation:

$$\begin{cases} \dfrac{\partial \rho}{\partial t} + \dfrac{\partial \rho u_j}{\partial x_j} = 0 \\ \dfrac{\partial \rho u_\iota}{\partial t} + \dfrac{\partial \rho u_j u_\iota}{\partial x_j} = -\dfrac{\partial P}{\partial x_\iota} + \dfrac{\partial \tau_{ij}}{\partial x_j} + \rho g_\iota + F_i^E \\ \dfrac{\partial \rho Y_\alpha}{\partial t} + \dfrac{\partial \rho u_j Y_\alpha}{\partial x_j} = -\dfrac{\partial F_{j,\alpha}}{\partial x_j} + \dot{r}_\alpha \\ \dfrac{\partial \rho h}{\partial t} + \dfrac{\partial \rho u_j h}{\partial x_j} = \dfrac{\partial P}{\partial t} - \dfrac{\partial}{\partial x_j}\left(F_{j,h} + u_i \tau_{ij}\right) - \dfrac{\partial q_j^r}{\partial x_j} + \rho u_i g_i \end{cases}$$

Some terms are unknown like diffusion heat and mass fluxes. They are modelled according to Fourier and Fick law and correspondingly. Newtonian fluid approach is used almost always due to almost all fluids behave this way (blood, for example, isn't a Newtonian fluid). In addition gas state equation is used as a closure equation. Radiation heat flux is modelled according to the radiation model that is not considered in this work.

There are different computational strategies to solve these equations. The first and the most obvious strategy is to solve these equations purely as they are. But this approach is enormously computational expensive as it requires very small grid resolution and time steps to resolve whole eddy spectra and collect enough statistics.

Other strategies are considered in the following sections.

2.2 Favre-Averaged Navier Stokes

This is another approach to calculate equations mentioned above. In this case we make time-averaging in specific time interval that is chosen to be longer than short-time turbulent pulsations and to be shorter than appreciable mean value alteration happens. The time-averaging is made through whole time-line if we have stationary problem. The averaging is made with density as weight function due to high density variations in the combustion-domain.

$$\overline{q(t)} = \lim_{T\to\infty} \frac{1}{T} \int_{t}^{t+T} q(s)ds \qquad\qquad \tilde{q} = \frac{\overline{\rho q}}{\overline{\rho}}$$

The first averaging is Reynolds averaging and the second is Favre-averaging. The following equation system is deduced after Favre-averaging:

$$\begin{cases} \dfrac{\partial \overline{\rho}}{\partial t} + \dfrac{\partial \overline{\rho}\tilde{u}_j}{\partial x_j} = 0 \\ \dfrac{\partial \overline{\rho}\tilde{u}_i}{\partial t} + \dfrac{\partial \overline{\rho}\tilde{u}_j\tilde{u}_i}{\partial x_j} = -\dfrac{\partial \overline{\rho}\,\widetilde{u_j'' u_i''}}{\partial x_j} - \dfrac{\partial \overline{P}}{\partial x_j} - \dfrac{\partial \overline{\tau}_{ij}}{\partial x_j} + \overline{\rho} g_i \\ \dfrac{\partial \overline{\rho}\tilde{Y}_\alpha}{\partial t} + \dfrac{\partial \overline{\rho}\tilde{u}_j\tilde{Y}_\alpha}{\partial x_j} = -\dfrac{\partial \overline{\rho}\,\widetilde{u_j'' Y_\alpha''}}{\partial x_j} - \dfrac{\partial \overline{F}_{j,\alpha}}{\partial x_j} + \overline{\dot{r}_\alpha} \\ \dfrac{\partial \overline{\rho}\tilde{h}}{\partial t} + \dfrac{\partial \overline{\rho}\tilde{u}_j\tilde{h}}{\partial x_j} = \dfrac{\partial \overline{P}}{\partial t} - \dfrac{\partial \overline{\rho}\,\widetilde{u_j'' h''}}{\partial x_j} - \dfrac{\partial}{\partial x_j}\left(\overline{F}_{j,h} + \overline{u_i \tau_{ij}}\right) - \dfrac{\partial \overline{q_j^r}}{\partial x_j} + \overline{\rho u_i} g_i \end{cases}$$

Some Favre-correlations are unknown and have to be modeled. Turbulent models are intended to do this work. They can introduce some empirical constants and functions or even solve additional transport equations. For example, almost all turbulent models make a Boussinesq hypothesis for relation between turbulent stress tensor and strain rate tensor. Turbulent mass and heat fluxes are modeled according to diffusion laws. Some additional variables are included in the system, such as turbulent viscosity, turbulent kinetic energy, turbulent dissipation rate, etc.

2.2.1 Spallart-Almaras turbulent model

This is one of the first turbulent models with one phenomenological transport equation for turbulent kinetic energy. This model was developed for specific external problems of aerodynamics, but later it was proved to give relatively good results for much wide spectra of tasks. The equation for turbulent kinetic viscosity is the following:

$$\frac{\partial \overline{\rho} v_t}{\partial t} + \frac{\partial \overline{\rho}\tilde{u}_j v_t}{\partial x_j} = \underbrace{\frac{1}{\sigma_{v_t}}\left[\frac{\partial}{\partial x_j}\left\{\left(\mu + \overline{\rho} v_t\right)\frac{\partial v_t}{\partial x_j}\right\} + C_{b2}\overline{\rho}\left(\frac{\partial v_t}{\partial x_j}\right)^2\right]}_{Diffusion} + \underbrace{C_{b1}\rho S_t v_t}_{Production} - \underbrace{C_{w1}\rho f_w\left(\frac{v_t}{d}\right)^2}_{Destruction} \qquad \mu_t = \rho v_t$$

2.2.1 K-ε turbulent models family

These are very widely used models with two additional transport equations for turbulent kinetic energy and turbulent dissipation rate. The first equation is strictly deduced from momentum transport equation, but there are lots of assumptions in deducing second equation. The family contains at least 3 relatives: Standard *k-ε* model, RNG *k-ε* model and Realizable *k-ε* model. First two differ only in the way of deducing: constants for the first model were obtained empirically, and for the second were obtained using Renormalized-Group Theory technique (Constants appear to be quite similar). The first and the last differ in one constant that is a function in the second model. These are the transport equations of these models:

$$\frac{\partial \bar{\rho} k}{\partial t} + \frac{\partial \bar{\rho} \tilde{u}_j k}{\partial x_j} = \frac{\partial}{\partial x_j}\left(\left(\mu + \frac{\mu_t}{\sigma_k}\right)\frac{\partial k}{\partial x_j}\right) - \underbrace{\bar{\rho}\,\widetilde{u_i'' u_j''}\frac{\partial \tilde{u}_i}{\partial x_j}}_{Turbulent\_stresses} - \underbrace{\frac{\mu_t}{\bar{\rho}}\frac{g_j}{\mathrm{Pr}_t}\frac{\partial \bar{\rho}}{\partial x_j}}_{gravity} - \underbrace{\bar{\rho} C_\mu k\omega}_{Dissipation}$$

$$\frac{\partial \bar{\rho} \varepsilon}{\partial t} + \frac{\partial \bar{\rho} \tilde{u}_j \varepsilon}{\partial x_j} = \underbrace{\frac{\partial}{\partial x_j}\left(\left(\mu + \frac{\mu_t}{\sigma_\varepsilon}\right)\frac{\partial \varepsilon}{\partial x_j}\right)}_{Turbulent\_diffusion} + \frac{\varepsilon}{k}\left(\underbrace{\bar{\rho}\,\widetilde{u_i'' u_j''}\frac{\partial \tilde{u}_i}{\partial x_j}}_{Turbulent\_stresses} + \underbrace{\frac{\mu_t}{\bar{\rho}}\frac{g_j}{\mathrm{Pr}_t}\frac{\partial \bar{\rho}}{\partial x_j}}_{gravity} + \underbrace{C_{\varepsilon 2}\bar{\rho}\varepsilon}_{Dissipation}\right)$$

2.2.2 K-ω turbulent models family

The *k-ε* model have a property to give good predictions in the far-from-walls zones, and to give not satisfying predictions in the near-wall regions. To make a model that would give good predictions in near-wall regions it was written another transport equation for specific dissipation rate instead of the equation for turbulent dissipation rate (Standard k-ω model). But this model gives bad predictions in far-from-walls zones. To improve this behavior a combination of k-ε and k-ω models is used according to the distance from the wall (Sheared Stress Tensor k-ω model).

$$\frac{\partial \bar{\rho} k}{\partial t} + \frac{\partial \bar{\rho} \tilde{u}_j k}{\partial x_j} = \frac{\partial}{\partial x_j}\left(\left(\mu + \frac{\mu_t}{\sigma_k}\right)\frac{\partial k}{\partial x_j}\right) - \underbrace{\bar{\rho}\,\widetilde{u_i'' u_j''}\frac{\partial \tilde{u}_i}{\partial x_j}}_{Turbulent\_stresses} - \underbrace{\frac{\mu_t}{\bar{\rho}}\frac{g_j}{\mathrm{Pr}_t}\frac{\partial \bar{\rho}}{\partial x_j}}_{gravity} - \underbrace{\bar{\rho} C_\mu k\omega}_{Dissipation}$$

$$\frac{\partial \bar{\rho} \omega}{\partial t} + \frac{\partial \bar{\rho} \tilde{u}_j \omega}{\partial x_j} = \frac{\partial}{\partial x_j}\left(\left(\mu + \frac{\mu_t}{\sigma_\omega}\right)\frac{\partial \omega}{\partial x_j}\right) - \alpha_1 \frac{\omega}{k}\left(\underbrace{\bar{\rho}\,\widetilde{u_i'' u_j''}\frac{\partial \tilde{u}_i}{\partial x_j}}_{Turbulent\_stresses} + \underbrace{\frac{\mu_t}{\bar{\rho}}\frac{g_j}{\mathrm{Pr}_t}\frac{\partial \bar{\rho}}{\partial x_j}}_{gravity}\right) - \underbrace{\bar{\rho}\beta_1\omega^2}_{Dissipation}$$

2.2.2 Reynolds Stress Model (RSM)

This model is designed for significantly anisotropic fluids. So each component of the turbulent stress tensor is modeled separatly by writing individual transport equation. The transport equation for turbulent disspation rate is aslo included in the system. This model is highly computational expensive and it is recommended to use it only for anisotropic flows.

2.3 Large-Eddy Simulation (LES)

This is the third approach of solving Navier-Stokes equations. It is located between DNS and RANS: only some part is averaged, but other part is simulated directly. It is the most modern technique, but it requieres lots of computational time so simulations are usually made on clusters.

In this model spatial averaging is used instead of time-averaging in Favre-Averaged Navier-Stokes. When a mesh is given it is quite easy to make spatial-averaging: the mean value of the variable in a cell is taken as a averaged variable value. Applying this averaging to Navier-Stokes equations we'll obtain another unknown corellations that are modeled using some sub-techniques. This approach resolves all large enough eddies directly (which characteristic scale is larger than mesh resolution), and sub-grid eddies are modeled due to averaging.

2.4 Chemistry models

The main purpose of chemistry models is to model reaction speed that is present in all species transport equations. Reaction speed of each component is net specie production/vanishing rate due to all chemical reactions. All chemistry models use stoichiometric coefficients of corresponding chemical reactions. And it must be kept in mind that reaction speed is highly-dependent on reactants and even products concentrations.

In the Laminar Finite-Rate Model specie production/vanishing rate is modeled as Arrhenius reaction source. In this model forward and backward rate constants are modeled using Arrhenius expression with Arrhenius exponent.

$$\hat{r}_{\alpha,r} = \left(\nu''_{\alpha,r} - \nu'_{\alpha,r}\right)\left(k_{f,r}\prod_{j=1}^{N} C_{j,r}^{\eta'_{j,r}} - k_{b,r}\prod_{j=1`}^{N} C_{j,r}^{\nu''_{j,r}}\right) \qquad k_{f,r} = A_r T^{\beta_r} e^{-E_r/RT}$$

In the Eddy-Dissipation (Eddy Break-up) Model an assumption of fast chemical reactions is used. So the reaction is fully controlled by turbulent mixing, this means that turbulence slowly mixes fuel and oxidizer into the reaction zone where they burn quickly. Also, the reaction rate can significantly decrease if the concentration of reaction products is very high. This happens due to significant decresement of the probaility of reaction between reactant moleculas (it is much harder for them to find the way to find each other).

$$\hat{r}_{\alpha,r} = \nu'_{\alpha,r} A \rho \frac{\varepsilon}{k} \min\left[\min_R\left(\frac{Y_R}{\nu'_{R,r} M_{w,R}}\right), B\frac{\sum_p Y_p}{\sum_j^N \nu''_{j,r} M_{w,j}}\right]$$

2.4 Non-premixed combustion approach

In this approach we refuse calculating all specie transport equations. It is very efficient for very complicated reaction mechanisms cases, where lots of calculations spend on species transport equations (even this amount of calculations can bring to instability). Another variable is defined for this approach and it is called mixture fraction. If the diffusion coefficients are equal for all species, then transport equation for mixture fraction could be deduced from any specie transport equation. And in every case it would be similar. The assumption of equal diffusion coefficients is significant, but in most cases it is acceptable. Another assumption is fast chemistry reactions. Mixture fraction appears to be conserved scalar.

$$f_\alpha = \frac{Z_\alpha - Z_{\alpha,ox}}{Z_{\alpha,fuel} - Z_{\alpha,ox}} \qquad \frac{\partial \bar{\rho}\tilde{f}}{\partial t} + \frac{\partial \bar{\rho}\tilde{u}_j \tilde{f}}{\partial x_j} = \frac{\partial}{\partial x_j}\left(\frac{\mu_t}{\sigma_t}\frac{\partial \tilde{f}}{\partial x_j}\right)$$

$$\frac{\partial \bar{\rho}\,\widetilde{f''^2}}{\partial t} + \frac{\partial \bar{\rho}\tilde{u}_j\,\widetilde{f''^2}}{\partial x_j} = \frac{\partial}{\partial x_j}\left(\frac{\mu_t}{\sigma_t}\frac{\partial\,\widetilde{f''^2}}{\partial x_j}\right) + C_g\mu_t\frac{\partial \tilde{f}}{\partial x_j}\frac{\partial \tilde{f}}{\partial x_j} - C_d\rho\frac{\varepsilon}{k}\widetilde{f''^2}$$

The last equation is written for mixture fraction fluctuations.

3 Measurement techniques

Characteristics of diffusion flames are usually obtained with the following laser techniques.

3.1 Raman-Rayleigh spectroscopy

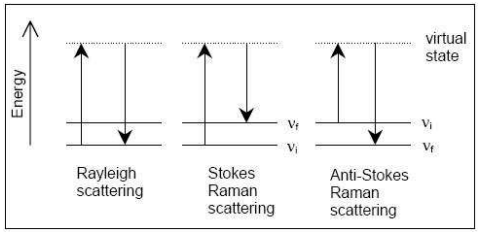

This technique is based on Raman-Rayleigh scattering effect. This effect in its turn is based on inelastic (with the frequency change) scattering of monochromatic light from a laser source.

The photon irradiates the sample and it could excite, remain in the same state or even return to the ground state. In this case photon is scattered, actually sample absorbs the photon and then reemits it. The frequency change in reemitted photon relatively to incident photon can:

1) Remain the same (Rayleigh scattering effect, 99.999%).
2) Decrease (Stokes Raman scattering effect, 0.001%).
3) Increase (Anti-Stokes Raman scattering effect).

The shift in the frequency reveals the fundamental properties and structure of the sample. So only Raman scattered photons are highly-informative. We can plot intensity of Raman scattered radiation as a function of the frequency shift from incident radiation (Raman shift). Each compound has a unique spectrum, which can easily distinguish different compounds from each other. This spectrum arises from molecular vibrations (natural sample frequency). These analysis is fast, easy and non-destructive.

3.2 Coherent Anti-Raman Stokes Spectroscopy

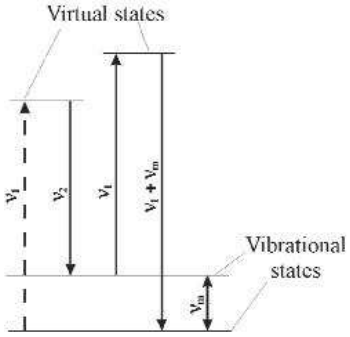

There are several non-linear techniques based on Raman-Rayleigh spectroscopy. Non-linearity is show itself on very high energies of incident radiation (very powerful lasers). In the case of non-linearity the amount of Raman scattered photons could increase up to 50% (impressive difference). The CARS technique is also based on this non-linear effect.

Two very strong collinear lasers are used in this technique. The frequency of the second laser is tuned up in the way that the frequency difference between the two lasers equals exactly the frequency of some Raman-active mode of interest. In this way we'll obtain highly intensive peak on Raman shift plot. But with this technique we can obtain only one peak of interest.

This technique also allows obtaining temperature of the sample. This is based on the dependence of the spectral shape of the CARS signature from temperature. With the increase of the temperature the spectral shape becomes rougher. It is explained this way: at low temperatures only the ground vibrational and rotational states are available. But as the temperature increases, higher vibrational and rotational state become available (more energy to make a jump) and populated. Spectral shape represents these processes.

3.2 Laser-Doppler Velocimetry

In this technique coherent light from a laser is split into two parallel beams that are then focused with a lens at the point where the velocity measurements are desired. There appears a trifling crossing region with few hundreds microns across and few millimeters long. At the point of interest these two beams interfere with each other to form interlacing bright and dark fringes.

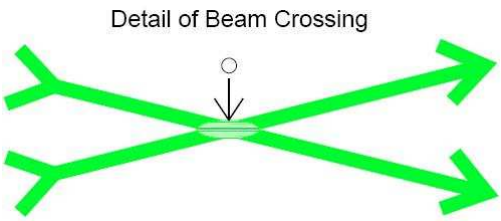

When a particle in the flow passes through these fringes it scatters a potion of incident light onto a photo detector. The resulting light signal contains the frequency proportional to the particle's velocity.

3 Intermediate results

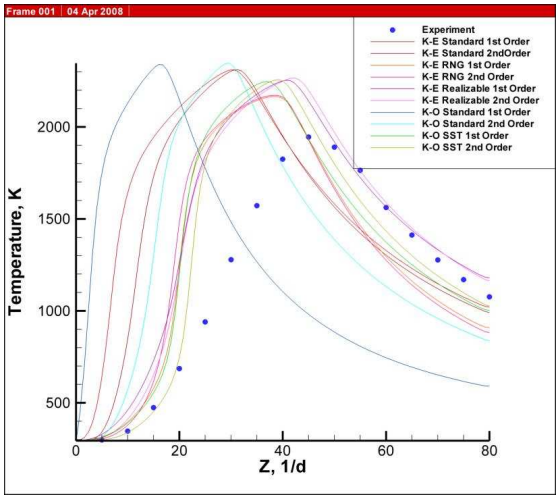

Temperature plot on symmetry axis

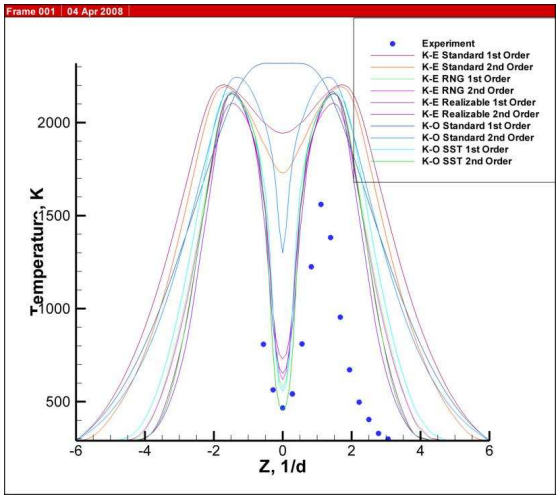

Temperature plot on radial line Z=15d

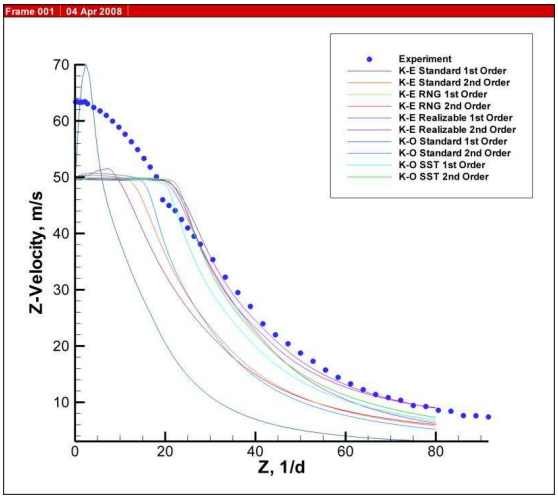

Z-Velocity plot on symmetry axis

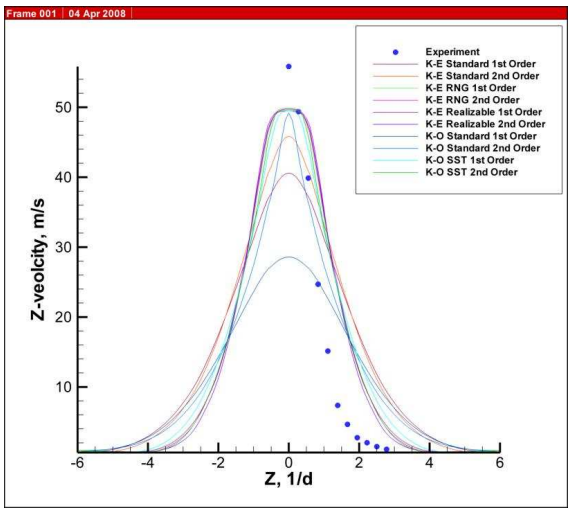

Z-Velocity plot on radial line Z=15d

On these plots experimental data is dotted. Lines correspond to different turbulent models with 2 equations. Models with one equation (Spallart-Allmaras) totally failed even in total absence of convergence. The worst models with two equations are k-ε Standart (1st order) and k-ω Standart (1st and 2nd order). The most adjacency showed k-ε Realizable (2nd order) and k-ω SST (1st and 2nd order). The global predictions of these models are as expected: the flame appears to be predicted shorter and wider. These are results without boundary velocity profile.

4 Conclusions and further improvements

First approaches obviously showed that these models are acceptable for engineering tasks. But these models are quite rough for the science tasks and detailed problem researches. So the next steps are the following:

1) Handle results for calculations with boundary profile velocity conditions.
2) Improve mesh and inspect changes (regions of significant changes).
3) Detail reaction mechanism and inspect changes
4) Test turbulence models with other radiation and chemistry models
5) Test solution on side boundary dependence
6) The main aim is to test more complex and more computational expensive model such as LES simulation